Quantum Simulation of Helium Hydride Cation in a Solid-State Spin Register

Ya Wang,*,† Florian Dolde,† Jacob Biamonte,*,‡ Ryan Babbush,¶,§ Ville Bergholm,‡ Sen Yang,† Ingmar Jakobi,† Philipp Neumann,† Alán Aspuru-Guzik,¶ James D. Whitfield,∥ and Jörg Wrachtrup*,†

†Third Institute of Physics, Research Center Scope and IQST, University of Stuttgart, 70569 Stuttgart, Germany, ‡ISI Foundation, Via Alassio 11/c, 10126 Torino, Italy, ¶Department of Chemistry and Chemical Biology, Harvard University, Cambridge, Massachusetts 02138 United States, §Google, 150 Main Street, Venice Beach, California 90291, United States, and ∥Department of Physics, Vienna Center for Quantum Science and Technology, University of Vienna, Boltzmanngasse 5, Vienna 1090, Austria

ABSTRACT *Ab initio* computation of molecular properties is one of the most promising applications of quantum computing. While this problem is widely believed to be intractable for classical computers, efficient quantum algorithms exist which have the potential to vastly accelerate research throughput in fields ranging from material science to drug discovery. Using a solid-state quantum register realized in a nitrogen-vacancy (NV) defect in diamond, we compute the bond dissociation curve of the minimal basis helium hydride cation, HeH^+. Moreover, we report an energy uncertainty (given our model basis) of the order of 10^{-14} hartree, which is 10 orders of magnitude below the desired chemical precision. As NV centers in diamond provide a robust and straightforward platform for quantum information processing, our work provides an important step toward a fully scalable solid-state implementation of a quantum chemistry simulator.

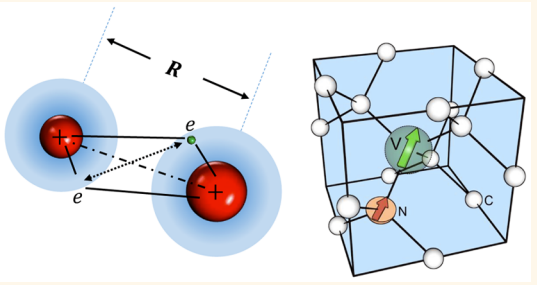

KEYWORDS: quantum simulation · electronic structure · molecular energy · diamond crystal · nitrogen-vacancy centers

Quantum simulation, as proposed by Feynman[1] and elaborated by Lloyd[2] and many others,[3−7] exploits the inherent behavior of one quantum system as a resource to simulate another quantum system. Indeed, there have been several experimental demonstrations of quantum simulators in various architectures including quantum optics, trapped ions, and ultracold atoms.[8] The importance of quantum simulators applied to electronic structure problems has been detailed in several recent review articles including refs 9−13 and promises a revolution in areas such as materials engineering, drug design, and the elucidation of biochemical processes.

The computational cost of solving the full Schrödinger equation of molecular systems using any known method on a classical computer scales exponentially with the number of atoms involved. However, it has been proposed that this calculation could be done efficiently on a quantum computer, with the cost scaling linearly in propagation time.[6] There is now a growing body of theoretical work proposing efficient quantum simulations of chemical Hamiltonians, *e.g.*, refs 14−24.

In contrast, experimental realizations of quantum simulations of quantum chemistry problems are still limited to small-scale demonstrations and are only performed in liquid-state NMR and photonic systems. First experiments demonstrated the simulation of the electronic structure of molecular hydrogen using quantum optics[15] and liquid-state NMR.[25] Recently, the energy of another molecule, the helium hydride cation, was calculated in a photonic system using a quantum variational eigensolver algorithm.[26] Besides the electronic structure, simulation of chemical reaction dynamics on an eight-site lattice was performed in NMR.[27]

Recently, the nitrogen-vacancy (NV) centers in diamond attracted significant attention due to its unique optical and spin

* Address correspondence to y.wang@physik.uni-stuttgart.de, jacob.biamonte@qubit.org, j.wrachtrup@physik.uni-stuttgart.de.

Received for review March 17, 2015 and accepted April 23, 2015.

Published online April 23, 2015
10.1021/acsnano.5b01651

properties.[28] The NV center consists of a substantial nitrogen atom at the carbon site and an adjacent vacancy. Its negative charge state forms a spin triplet ground state, with $m_s = 0$ and $m_s = \pm 1$ sublevels that are separated by a zero-field splitting of $D \approx 2.87$ GHz. This spin system can be initialized and read out via optical pumping and spin-dependent fluorescence. The NV center therefore does not suffer from signal losses with increasing system size like NMR and avoids challenges such as the need for high-fidelity single-photon sources and detectors that are still beyond the present capabilities in optical quantum systems.[29] Progress to date demonstrates that the NV centers are among the most accurate and most controllable candidates for quantum information processing.[30−41] Milestone demonstrations include high-fidelity initialization and readout,[30−33] heralded generation of entanglement,[33−38] implementation of quantum control,[38,42,43] ultralong spin coherence time,[40] nonvolatile memory,[41] quantum error correction,[33,39] as well as a host of metrology and sensing experiments.[44,45] Several proposals to scale up the size of NV systems currently exist, *e.g.*, refs 38 and 46. This makes the NV center an ideal candidate for a scalable quantum simulator.

Here, we demonstrate the quantum simulation of an electronic structure with the NV center at ambient conditions. We use a quantum phase estimation algorithm[47] to enhance the simulations precision. Our experimentally computed energy agrees well with the corresponding classical calculations within chemical precision and a deviation of 1.4×10^{-14} hartree. Furthermore, we obtain the molecular electronic potential energy surfaces by performing the simulation for different distances of the atoms.

RESULTS AND DISCUSSION

The chemical system we consider in this paper is the helium hydride cation, HeH^+ (Figure 1a), believed to be the first molecule in the early universe.[48] While HeH^+ is isoelectronic (i.e., has the same number of electrons) with the previously studied molecular hydrogen, the reduced symmetry requires that we simulate larger subspaces of the full configuration interaction (FCI) Hamiltonian H_{sim}. Specifically, we consider

$$H_{sim} = T_e + W_{ee} + V_{eN}(R) + E_N(R) \qquad (1)$$

in a minimal single particle basis with one site per atom. Here, T_e and W_{ee} are the kinetic and Coulomb operators for the electrons, V_{eN} is the electron−nuclear interaction, and E_N is the nuclear energy due to the Coulomb interaction between the hydrogen and the helium atom. The last two terms depend on the internuclear distance R.

In this work, we consider the singlet ($S = 0$) sector of the electronic Hamiltonian in a minimal single-electron basis consisting of a single site at each atom given by

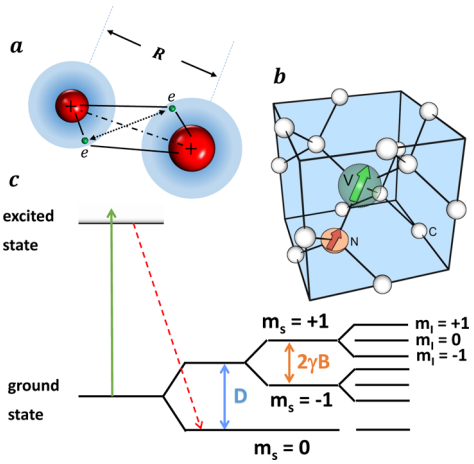

Figure 1. Calculation of HeH^+ molecular energy with NV spin register in diamond. (a) HeH^+, molecule to be simulated. It consists of a hydrogen and a helium nucleus and two electrons. The distance (bond length) between the nuclei is denoted by *R*. Dot-dashed line, straight line, and dotted arrows indicate the nucleus−nucleus, electron−nucleus, and electron−electron Coulomb interactions, respectively. (b) Nitrogen-vacancy center in diamond, used as a quantum simulator. The electron spin is used for simulation and the nuclear spin as the probe qubit for energy readout. (c) Energy level diagram for the coupled spin system formed by the NV electron spin and associated ^{14}N nuclear spin. Optical transitions between ground and excited state are used to initialize and measure the electron spin state.

contracted Gaussian orbitals. After taking symmetries into account, the Hamiltonian can be represented as a 3×3 matrix in the basis $(\Psi_1, \Psi_6, {}^1/_{2^{1/2}}(\Psi_3 - \Psi_4))$. Each term of the Hamiltonian in the single particle basis (*e.g.*, $\langle\chi_i|(T_e + V_{eN})\ |\chi_j\rangle$) is precomputed classically at each internuclear separation R using the canonical spin orbitals found via the Hartree−Fock (HF) procedure which often scales as a third order polynomial in the number of basis functions.

After obtaining H_{sim} through this (typically) efficient classical computation, we perform the quantum simulation of this molecule on a single-NV register, which consists of an electronic spin-1 and an associated ^{14}N nuclear spin-1 forming a qutrit pair (Figure 1b). The electronic spin-1 of the NV system acts as the *simulation register* through mapping the molecular basis $(\Psi_1, \Psi_6, {}^1/_{2^{1/2}}(\Psi_3 - \Psi_4))$ onto its $m_s = (1, 0, -1)$ states. Such a compact mapping is more efficient in that the states of simulated system and of the simulation system are simply enumerated and equated. The ^{14}N nuclear spin-1 is used as the *probe register* to read out the energies using the iterative phase estimation algorithm (IPEA),[47] as shown in Figure 1c. The simulation is realized by three steps: (i) preparation of the system into an ansatz state $|\psi\rangle$, which is close to an eigenstate of the simulated Hamiltonian H_{sim}; (ii) evolution of the simulation register under the molecular Hamiltonian H_{sim} to generate phase shift on the probe register; and (iii) readout of the phase shift on the probe register to extract the molecular energy (Figure 2a).

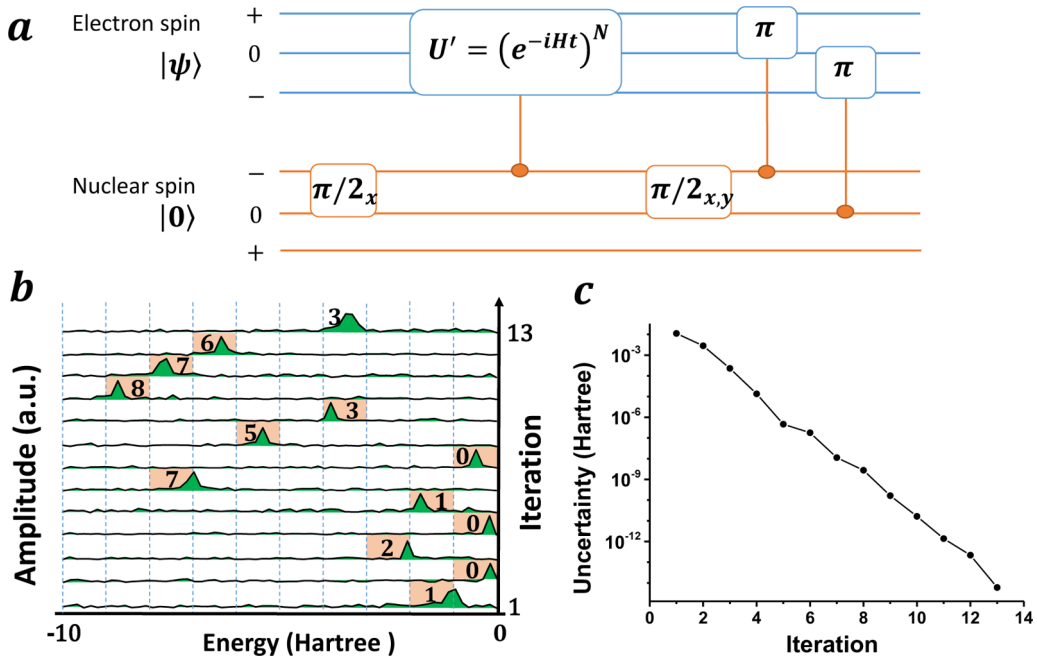

Figure 2. Energy readout through quantum phase estimation algorithm. (a) Experimental implementation of the IPEA algorithm. The controlled gate U' is realized using optimal control. The x, y phases in the last $\pi/2$ pulse measure the real and imaginary parts of the signal, respectively, which yield the sign of the measured energy. The number of repetitions $N = 10^{k-1}$ depends on the iteration k. (b) Experimental results of iterative phase estimation algorithm to enhance the precision of measured energy for the case of $R = 90$ pm. The Fourier spectrum of the first iteration ($k = 1$) fixes the energy roughly between -10 and 0 hartree. The precision is then improved iteratively by narrowing down the energy range. In each iteration, the energy range is divided into 10 equal segments. The red area indicates the energy range for the next iteration. After each iteration at least one decimal digit, denoted by the number in the red area, is resolved. Note that the value here is offset by $\mathrm{tr}(H_{\mathrm{sim}})/3$ (see the Supporting Information for details). (c) The uncertainty of the measured energy as a function of the iteration number.

In the first step, an ansatz state is prepared that has an overlap with the corresponding eigenstate $|e_n\rangle$ that decreases at most polynomially as the system size grows. The phase estimation algorithm[49] can then be used to project the ansatz state into the exact eigenstate with sufficiently high probability. One possible approach to realize this requirement is to use adiabatic state preparation,[14,25,50] the performance of which depends on the energy gap during the entire evolution process. An alternative approach is to approximate the eigenstate with a trial state. In our demonstration, the simulation register is initialized in a trial state $|\tau\rangle \in \{|+1\rangle, |-1\rangle\}$. Each state is easily found to be close to one eigenstate of the molecular Hamiltonian H_{sim} by looking at its matrix representation. In more general cases such trial states can often be prepared based on classical approximate methods. The probe register is first initialized into state $|0\rangle$ and then prepared in the superposition state $|\psi(0)\rangle = (|0\rangle + |-1\rangle)/2^{1/2}$ through a $\pi/2$ pulse to obtain a phase shift in the evolution.

In the next step, a controlled-$U(t)$ gate for different times t, where $U(t) = \exp(-i\, H_{\mathrm{sim}}\, t)$, is applied on the simulation register to encode the energies into a relative phase of the probe register, resulting in the state

$$|\psi(t)\rangle = \frac{1}{\sqrt{2}}\sum_k a_k(|0\rangle + \mathrm{e}^{-iE_k t}|\ -1\rangle)|e_k\rangle \qquad (2)$$

where the trial state is expressible as a superposition of all the H_{sim} eigenstates $|\tau\rangle = \sum_k a_k|e_k\rangle$. The reduced density matrix of the probe register

$$\rho_{\mathrm{probe}}(t) = \frac{1}{2}\begin{pmatrix} 1 & \sum_k |a_k|^2 \mathrm{e}^{-iE_k t} \\ \sum_k |a_k|^2 e^{iE_k t} & 1 \end{pmatrix} \qquad (3)$$

obtains a phase shift (off-diagonal elements) that contains the information about the energies. Finally, the phase information is transferred to the electron spin for readout by a nuclear spin $\pi/2$-pulse, followed immediately by selective π-pulses on the electron spin. To measure the energy precisely, we perform a classical Fourier analysis on the signal for different evolution times (t_s, $2t_s$, ..., Lt_s). This readout method can help to resolve the probability $|a_k|^2$ of each eigenstate $|e_k\rangle$ and approximate the corresponding energy E_k. We choose t_s such that the sampling rate $^1/_{t_s} > |E_n|/\pi$. An example for the experimental Fourier spectrum are shown in Figure 2b. The position of the peak indicates the eigenvalue of the molecular Hamiltonian.

To enhance the precision of the energy eigenvalues, an iterative phase estimation algorithm is performed. A central feature of this algorithm includes repeating the unitary operator U to increase readout precision. Expressing the energy as a string of decimal digits, $E_k = x_1, x_2, x_3$ ..., the first digit x_1 can be determined by the

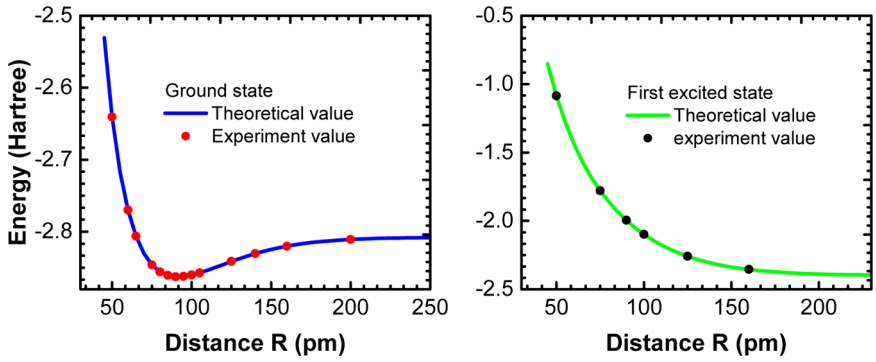

Figure 3. Energy surfaces of the HeH^+ molecule. The energy surface of the second excited state can be obtained by subtracting energies of the ground and first excited states from the trace of H_{sim} and is not shown. All of the measured energies are obtained in five iterations.

first-round phase estimation process. Once x_1 is known, the second digit x_2 can be iteratively determined by implementing the unitary operator U^p, where $p = 10$. For the k^{th} iteration, $p = 10^{k-1}$. An increasingly precise energy can be obtained through continued iterations. However, in practice, the repetitions and therefore the iterations are fundamentally limited by the coherence time of the quantum system. Moreover, the accumulated gate errors become a dominant limitation of the energy precision as the repetitions increase. To avoid such shortcomings, in our demonstration the time evolution operators U^p are realized and optimized with optimal control theory, which can overcome several difficult features found when scaling up the register size.[38] Although it cannot be applied in large registers to generate the quantum gates directly, it can be used to generate flexible smaller building blocks, ensuring high-fidelity control in future large-scale applications. In the present case, the method is unscalable because we compute the unitary propagator using a classical computer. However, by using a Trotter-type gate sequence to implement the propagators, *e.g.*,[16] this can be designed with polynomially scaling.

Figure 2b,c show the results of such an iterative process in the case of internuclear distance $R = 90$ pm with trial state $|+1\rangle$. As the iterations increase, more precise decimal digits of the ground-state energy are resolved. After 13 repetitions, the molecular energy, with an offset $\mathrm{tr}(H_{sim})/3$, is extracted to be $-1.020170538763387 \pm 8 \times 10^{-15}$ hartree, very close to the theoretical value, which is -1.020170538763381 hartree, with an uncertainty of $\pm 1.4 \times 10^{-14}$ hartree. To the best of knowledge, our results are four times more accurate than the previous record.[25]

Once the energies have been measured, we can obtain the potential energy surface of the molecule by repeating the procedure for different distances R (Figure 3). The ground-state energy surface is obtained with the trial state $|+1\rangle$, and the first excited state energy surface is obtained with the trial state $|-1\rangle$. We obtain the remaining eigenenergy (of the second excited state) without further measurement by subtracting the ground and first excited-state energies from the trace of H_{sim}. The potential energy surfaces can be used to compute key molecular properties such as ionization energies and vibrational energy levels. An important example is the equilibrium geometry: we found the minimal energy for the ground state, -2.86269 hartree, at a bond length of 91.3 pm. In addition, we obtained a binding energy of 0.07738 hartree in our basis.

To improve the accuracy of our results we would need to simulate the system in a larger basis. Recent advances in this direction show that we can enlarge the size of the NV spin system by either including more coupled nuclear spins associated with single NV electron spin[33,39] or correlating several electron spins mediated through optical photons[37] or through magnetic interactions between them.[36] The former method is able to provide ~6 nuclear spins for single NV node, and the latter method currently is limited to two electron spins.[36,37] In both hybrid-spin systems the control is shown to be universal.[33,36,37,39] Combining these two methods in principle could enlarge the NV system to a 10-qubit quantum processor which is enough to perform more complicated tasks. In these large systems, the simulated propagators can be implemented using Trotter sequences and should be accompanied by error correction. Optimal control methods, as we have demonstrated here, should prove necessary to perform these tasks with satisfactory precision.

CONCLUSION

We have demonstrated the most precise quantum simulation of molecular energies to date, which represents an important step toward the advanced level of control required by future quantum simulators that will outperform classical methods. The energies we obtained for the helium hydride cation surpass chemical precision by 10 orders of magnitude (with respect to the basis). The accuracy of our results can be increased by using a larger, more flexible single-particle basis set, but this will require a larger quantum simulator that eventually will require error correction schemes.[18]

Our study presents evidence that quantum simulators can be controlled well enough to recover increasingly precise data. The availability of highly accurate energy eigenvalues of large molecules is presently far out of reach of existing computational technology, and quantum simulation could open the door to a vast range of new technological applications. The approach we took was based on iterative phase estimation[47] and optimal control decompositions[38]—these will form key building blocks for any solid-state quantum simulator. Even more generally, this study would suggest that the techniques presented here should be employed in any future simulator that will outperform classical simulations of electronic structure calculations.

METHODS.

Computation of Molecular Hamiltonians. The full configuration interaction Hamiltonian is a sparse matrix, and each matrix element can be computed in polynomial time. The N-electron Hamiltonian is asymotpically sparse. For a basis set with M orbitals, there are M^4 terms in the Hamiltonian but the Hamiltonian is of size $((M!)/(N!\ (M-N)!)) \approx M^N$ which is exponential as the number of electrons grow. To generate the Hamiltonian, we fix the nuclear configuration and then compute the necessary one- and two-body integrals which parametrize the FCI matrix at each fixed bond length in the standard STO-3G basis,[51] using the PSI3 electronic structure package.[52] The minimal basis HeH^+ system has two spatial orbitals which we denote as $g(r)$ and $e(r)$ and two spin functions denoted as $\alpha(\sigma)$ and $\beta(\sigma)$ which are eigenstates of the S_z operator. We combine these to form four spin orbitals, $\chi_1 = g(r)\ \alpha(r)$, $\chi_2 = g(r)\ \beta(\sigma)$, $\chi_3 = e(r)\ \alpha(\sigma)$, and $\chi_4 = e(r)\ \beta(\sigma)$. There are six possible two-electron Slater determinants, $\Psi_1 = \mathcal{A}(\chi_1\chi_2)$, $\Psi_2 = \mathcal{A}(\chi_1\chi_3)$, $\Psi_3 = \mathcal{A}(\chi_1\chi_4)$, $\Psi_4 = \mathcal{A}(\chi_2\chi_3)$, $\Psi_5 = \mathcal{A}(\chi_2\chi_4)$, and $\Psi_6 = \mathcal{A}(\chi_3\chi_4)$. More explicitly

$$\mathcal{A}(\chi_i\chi_j) = \frac{1}{\sqrt{2}}\begin{vmatrix} \chi_i(r_1\sigma_1) & \chi_j(r_1\sigma_1) \\ \chi_i(r_2\sigma_2) & \chi_j(r_2\sigma_2) \end{vmatrix} \quad (4)$$

States Ψ_1, Ψ_3, Ψ_4, and Ψ_6 have total projected spin of $M_z = 0$, whereas Ψ_2 and Ψ_5 have projected values of $M_z = 1$ and $M_z = -1$ respectively. Only Ψ_1 and Ψ_6 are valid eigenstates of the total spin operator S^2; however, the symmetric and antisymmetric combinations of Ψ_3 and Ψ_4 yield the $m_s = 0$ triplet and an additional singlet, respectively. When a computation is requested on the singlet state, the PSI3 package computes the symmetry-adapted FCI matrix in the basis of Ψ_1, Ψ_3, Ψ_4, and Ψ_6. By combining Ψ_3 and Ψ_4 we obtained the three HeH^+ singlet states used in this experiment: Ψ_1, Ψ_6, and $^1/_{2^{1/2}}(\Psi_3 - \Psi_4)$.

Sample Characteristics. We use a NV in high-purity diamond grown by microwave-assisted chemical vapor deposition (CVD). The intrinsic nitrogen content of the grown crystal is below 1 ppb, and the ^{12}C content is enriched to 99.9%. Experiments are performed at room temperature with an applied magnetic field of 11 gauss. The electron spin's coherence times are $T_2^* \approx 80\ \mu s$ and $T_2 \approx 600\ \mu s$, while the nuclear spin's coherence time is limited by the relaxation time of the electron spin (on the order of milliseconds).

Controlled $U^*(t)$ Gate Realization. To calculate $U^*(t)$, we use the gradient ascent pulse engineering (GRAPE) algorithm to optimize the pulse sequence, with the final fidelity always larger than 0.99. For every controlled gate, the pulse sequence consists of 10 pieces of 140 ns each. Two microwave frequencies are applied simultaneously to control the electron spin, in the observed hyperfine peaks of the $|m_I = -1, m_s = 0\rangle \rightarrow |m_I = -1, m_s = +1\rangle$ and $|m_I = -1, m_s = 0\rangle \rightarrow |m_I = -1, m_s = -1\rangle$ transitions.

Conflict of Interest: The authors declare no competing financial interest.

Acknowledgment. V.B. and J.D.B. acknowledge financial support by Fondazione Compagnia di San Paolo through the Q-ARACNE project. J.D.B. acknowledges the Foundational Questions Institute (under Grant No. FQXi-RFP3-1322) for financial support. R.B. and A.A.-G. acknowledge support from the Air Force Office of Scientific Research under contract FA9550-12-1-0046, as well as the National Science Foundation CHE-1152291 and the Corning Foundation. J.W. acknowledges support by the EU via IP SIQS and the ERC grant SQUTEC as well as the DFG via the research group 1493 and SFB/TR21 and the Max Planck Society. J.D.W. thanks the VCQ and Ford postdoctoral fellowships for support. We thank Mauro Faccin and Jacob Turner for providing valuable feedback regarding the manuscript.

Supporting Information Available: Detailed information about the initialization of spin register and realization of controlled gate are provided. The Supporting Information is available free of charge on the ACS Publications website at DOI: 10.1021/acsnano.5b01651.

REFERENCES AND NOTES

1. Feynman, R. P. Simulating Physics with Computers. *Int. J. Theor. Phys.* **1982**, *21*, 467–488.
2. Lloyd, S. Universal Quantum Simulators. *Science* **1996**, *273*, 1073–1078.
3. Wiesner, S. Simulations of Many-Body Quantum Systems by a Quantum Computer. *ArXiv: quant-ph/9603028* **1996**.
4. Zalka, C. Efficient Simulation of Quantum Systems by Quantum Computers. *Fortschr. Phys.* **1998**, *46*, 877–879.
5. Abrams, D. S.; Lloyd, S. Simulation of Many-Body Fermi Systems on a Universal Quantum Computer. *Phys. Rev. Lett.* **1997**, *79*, 2586–2589.
6. Berry, D. W.; Ahokas, G.; Cleve, R.; Sanders, B. C. Efficient Quantum Algorithms for Simulating Sparse Hamiltonians. *Commun. Math. Phys.* **2007**, *270*, 359–371.
7. Georgescu, I.; Brown, S. E.; Mandelshtam, V. A. Mapping The Phase Diagram for Neon to a Quantum Lennard-Jones Fluid Using Gibbs Ensemble Simulations. *J. Chem. Phys.* **2013**, *138*, 134502.
8. Trabesinger, A. Quantum Simulation. *Nat. Phys.* **2012**, *8*, 263–263.
9. Yung, M.-H., Whitfield, J. D., Boixo, S., Tempel, D. G., Aspuru-Guzik, A. *Quantum Information and Computation for Chemistry*; Advances in Chemical Physics; John Wiley & Sons, Inc.: New York, 2014; Vol. 154, pp 67−106.
10. Kassal, I.; Whitfield, J. D.; Perdomo-Ortiz, A.; Yung, M.-H.; Aspuru-Guzik, A. Simulating Chemistry Using Quantum Computers. *Annu. Rev. Phys. Chem.* **2011**, *62*, 185–207.
11. Brown, K. L.; Munro, W. J.; Kendon, V. M. Using Quantum Computers for Quantum Simulation. *Entropy* **2010**, *12*, 2268–2307.
12. Lu, D.; Xu, B.; Xu, N.; Li, Z.; Chen, H.; Peng, X.; Xu, R.; Du, J. Quantum Chemistry Simulation on Quantum Computers: Theories and Experiments. *Phys. Chem. Chem. Phys.* **2012**, *14*, 9411–9420.
13. Georgescu, I. M.; Ashhab, S.; Nori, F. Quantum Simulation. *Rev. Mod. Phys.* **2014**, *86*, 153–185.
14. Aspuru-Guzik, A.; Dutoi, A. D.; Love, P. J.; Head-Gordon, M. Simulated Quantum Computation of Molecular Energies. *Science* **2005**, *309*, 1704–1707.
15. Lanyon, B. P.; Whitfield, J. D.; Gillet, G. G.; Goggin, M. E.; Almeida, M. P.; Kassal, I.; Biamonte, J. D.; Mohseni, M.; Powell, B. J.; Barbieri, M.; et al. Towards Quantum Chemistry on a Quantum Computer. *Nat. Chem.* **2010**, *2*, 106–111.
16. Whitfield, J. D.; Biamonte, J.; Aspuru-Guzik, A. Simulation of Electronic Structure Hamiltonians Using Quantum Computers. *Mol. Phys.* **2010**, *2*, 106–111.

17. Kassal, I.; Whitfield, J. D.; Perdomo-Ortiz, A.; Yung, M.-H.; Aspuru-Guzik, A. Simulating Chemistry Using Quantum Computers. *Annu. Rev. Phys. Chem.* **2010**, *62*, 185–207.
18. Cody Jones, N.; Whitfield, J. D.; McMahon, P. L.; Yung, M.-H.; Meter, R. V.; Aspuru-Guzik, A.; Yamamoto, Y. Faster Quantum Chemistry Simulation on Fault-Tolerant Quantum Computers. *New J. Phys.* **2012**, *14*, 115023(1−35).
19. Wecker, D.; Bauer, B.; Clark, B. K.; Hastings, M. B.; Troyer, M. Can Quantum Chemistry Be Performed on a Small Quantum Computer? *ArXiv: 1312.1695*, **2013**.
20. Toloui, B.; Love, P. J. Quantum Algorithms for Quantum Chemistry Based on the Sparsity of the CI-Matrix. *ArXiv: 1312.2579*, **2013**.
21. Hastings, M. B., Wecker, D.; Bauer, B.; Troyer, M. Improving Quantum Algorithms for Quantum Chemistry. *ArXiv: 1403.1539*, **2014**.
22. Veis, L.; Pittner, J. Quantum Computing Applied to Calculations of Molecular Energies: CH2 Benchmark. *J. Chem. Phys.* **2010**, *133*, 194106.
23. Veis, L.; Višňák, J.; Fleig, T.; Knecht, S.; Saue, T.; Visscher, L.; Pittner, J. c. v. Relativistic Quantum Chemistry on Quantum Computers. *Phys. Rev. A* **2012**, *85*, 030304.
24. Veis, L.; Pittner, J. Adiabatic State Preparation Study of Methylene. *J. Chem. Phys.* **2014**, *140*, 214111.
25. Du, J.; Xu, N.; Peng, X.; Wang, P.; Wu, S.; Lu, D. NMR Implementation of a Molecular Hydrogen Quantum Simulation with Adiabatic State Preparation. *Phys. Rev. Lett.* **2010**, *104*, 030502.
26. Peruzzo, A., McClean, J., Shadbolt, P., Yung, M.-H., Zhou, X.-Q., Love, P. J., Aspuru-Guzik, A., OBrien, J. L. A Variational Eigenvalue Solver on a Photonic Quantum Processor *Nat. Commun.* **2014**, *5*.
27. Lu, D.; Xu, N.; Xu, R.; Chen, H.; Gong, J.; Peng, X.; Du, J. Simulation of Chemical Isomerization Reaction Dynamics on a NMR Quantum Simulator. *Phys. Rev. Lett.* **2011**, *107*, 020501.
28. Doherty, M. W.; Manson, N. B.; Delaney, P.; Jelezko, F.; Wrachtrup, J.; Hollenberg, L. C. L. The Nitrogen-Vacancy Colour Centre in Diamond. *Phys. Rep.* **2013**, *528*, 1–45.
29. Kok, P.; Munro, W.; Nemoto, K.; Ralph, T.; Dowling, J.; Milburn, G. Linear Optical Quantum Computing with Photonic Qubits. *Rev. Mod. Phys.* **2007**, *79*, 135–174.
30. Gruber, A.; Dräbenstedt, A.; Tietz, C.; Fleury, L.; Wrachtrup, J.; von Borczyskowski, C. Scanning Confocal Optical Microscopy and Magnetic Resonance on Single Defect Centers. *Science* **1997**, *276*, 2012–2014.
31. Neumann, P.; Beck, J.; Steiner, M.; Rempp, F.; Fedder, H.; Hemmer, P. R.; Wrachtrup, J.; Jelezko, F. Single-Shot Readout of a Single Nuclear Spin. *Science* **2010**, *329*, 542–544.
32. Robledo, L.; Childress, L.; Bernien, H.; Hensen, B.; Alkemade, P. F. a.; Hanson, R. High-Fidelity Projective Read-Out of a Solid-State Spin Quantum Register. *Nature* **2011**, *477*, 574–578.
33. Waldherr, G.; Wang, Y.; Zaiser, S.; Jamali, M.; Schulte-Herbrüggen, T.; Abe, H.; Ohshima, T.; Isoya, J.; Du, J. F.; Neumann, P.; et al. Quantum Error Correction in a Solid-State Hybrid Spin Register. *Nature* **2014**, *506*, 204–207.
34. Neumann, P.; Mizuochi, N.; Rempp, F.; Hemmer, P.; Watanabe, H.; Yamasaki, S.; Jacques, V.; Gaebel, T.; Jelezko, F.; Wrachtrup, J. Multipartite Entanglement Among Single Spins in Diamond. *Science* **2008**, *320*, 1326–1329.
35. Togan, E.; Chu, Y.; Trifonov, A. S.; Jiang, L.; Maze, J.; Childress, L.; Dutt, M. V. G.; Sorensen, A. S.; Hemmer, P. R.; Zibrov, A. S.; et al. Quantum Entanglement Between an Optical Photon and a Solid-State Spin Qubit. *Nature* **2010**, *466*, 730.
36. Dolde, F.; Jakobi, I.; Naydenov, B.; Zhao, N.; Pezzagna, S.; Trautmann, C.; Meijer, J.; Neumann, P.; Jelezko, F.; Wrachtrup, J. Room-Temperature Entanglement Between Single Defect Spins in Diamond. *Nat. Phys.* **2013**, *8*, 1–5.
37. Bernien, H.; Hensen, B.; Pfaff, W.; Koolstra, G.; Blok, M. S.; Robledo, L.; Taminiau, T. H.; Markham, M.; Twitchen, D. J.; Childress, L.; et al. Heralded Entanglement Between Solid-State Qubits Separated by Three Metres. *Nature* **2013**, *497*, 86–90.
38. Dolde, F.; Bergholm, V.; Wang, Y.; Jakobi, I.; Naydenov, B.; Pezzagna, S.; Meijer, J.; Jelezko, F.; Neumann, P.; Schulte-Herbrüggen, T.; et al. High Fidelity Spin Entanglement Using Optimal Control. *Nat. Commun.* **2014**, *5*, 3371.
39. Taminiau, T. H.; Cramer, J.; van der Sar, T.; Dobrovitski, V. V.; Hanson, R. Universal Control and Error Correction in Multi-Qubit Spin Registers in Diamond. *Nat. Nanotechnol.* **2014**, 1–7.
40. Balasubramanian, G.; Neumann, P.; Twitchen, D.; Markham, M.; Kolesov, R.; Mizuochi, N.; Isoya, J.; Achard, J.; Beck, J.; Tissler, J.; et al. Ultralong Spin Coherence Time in Isotopically Engineered Diamond. *Nat. Mater.* **2009**, *8*, 383–387.
41. Maurer, P. C.; Kucsko, G.; Latta, C.; Jiang, L.; Yao, N. Y.; Bennett, S. D.; Pastawski, F.; Hunger, D.; Chisholm, N.; Markham, M.; et al. Room-Temperature Quantum Bit Memory Exceeding One Second. *Science* **2012**, *336*, 1283–1286.
42. Jelezko, F.; Gaebel, T.; Popa, I.; Domhan, M.; Gruber, A.; Wrachtrup, J. Observation of Coherent Oscillation of a Single Nuclear Spin and Realization of a Two-Qubit Conditional Quantum Gate. *Phys. Rev. Lett.* **2004**, *93*, 130501.
43. Dutt, M. V. G.; Childress, L.; Jiang, L.; Togan, E.; Maze, J.; Jelezko, F.; Zibrov, A. S.; Hemmer, P. R.; Lukin, M. D. Quantum Register Based on Individual Electronic and Nuclear Spin Qubits in Diamond. *Science* **2007**, *316*, 1312–1316.
44. Taylor, J. M.; Cappellaro, P.; Childress, L.; Jiang, L.; Budker, D.; Hemmer, P. R.; Yacoby, A.; Walsworth, R.; Lukin, M. D. High-sensitivity diamond magnetometer with nanoscale resolution. *Nat. Phys.* **2008**, *4*, 29.
45. Doherty, M. W.; Struzhkin, V. V.; Simpson, D. A.; McGuinness, L. P.; Meng, Y.; Stacey, A.; Karle, T. J.; Hemley, R. J.; Manson, N. B.; Hollenberg Lloyd C, L.; et al. Electronic Properties and Metrology Applications of the Diamond NV Center under Pressure. *Phys. Rev. Lett.* **2014**, *112*, 47601.
46. Bermudez, A.; Jelezko, F.; Plenio, M. B.; Retzker, A. Electron-Mediated Nuclear-Spin Interactions between Distant Nitrogen-Vacancy Centers. *Phys. Rev. Lett.* **2011**, *107*, 150503.
47. Parker, S.; Plenio, M. B. Efficient Factorization with a Single Pure Qubit and log N Mixed Qubits. *Phys. Rev. Lett.* **2000**, *85*, 3049–3052.
48. Engel, E. A.; Doss, N.; Harris, G. J.; Tennyson, J. Calculated Spectra for HeH+ and Its Effect on the Opacity of Cool Metal-Poor Stars. *Mon. Not. R. Astron. Soc.* **2005**, *357*, 471–477.
49. Kitaev, A. Y., Shen, A. H., Vyalyi, M. N. *Classical and Quantum Computation*; Graduate Studies in Mathematics; American Mathematical Society: Providence, RI, 2002; Vol. 47.
50. Biamonte, J. D.; Bergholm, V.; Whitfield, J. D.; Fitzsimons, J.; Aspuru-Guzik, A. Adiabatic Quantum Simulators. *AIP Adv.* **2011**, *1*, 022126.
51. Hehre, W. J.; Stewart, R. F.; Pople, J. A. Self-Consistent Molecular Orbital Methods I. Use of Gaussian Expansions of Slater-Type Atomic Orbitals. *J. Chem. Phys.* **1969**, *51*, 2657–2664.
52. Crawford, T. D.; Sherrill, C. D.; Valeev, E. F.; Fermann, J. T.; King, R. A.; Leininger, M. L.; Brown, S. T.; Janssen, C. L.; Seidl, E. T.; Kenny, J. P.; et al. PSI3: An Open-Source Ab Initio Electronic Structure Package. *J. Comput. Chem.* **2007**, *28*, 1610–1616.